Organic-inorganic hybrid nanostructured materials for photovoltaics and solar fuels

Lai, Lai-Hung

6

Near-infrared Light Harvesting by Incorporating Carbon Nanotubes into Organic-inorganic Hybrid Blends for Photoelectrochemical Hydrogen Production

In this chapter, we demonstrate that the incorporation of semiconducting single-walled carbon nanotubes (s-SWNT) into hybrid photocathode composed by QDs and conjugated polymers can extend the light absorption range from the visible to the near-infrared (NIR) spectral range, leading to improved photoelectrochemical (PEC) properties. Furthermore, s-SWNTs have the tendency to form a mesoporous "scaffold" in the hybrid blend, enlarging the surface area of photocathode for proton reduction, resulting in better device performance. *EQE* of 30% in the visible and 1.5% in the NIR were obtained in samples fabricated with s-SWNT "scaffolds".*

*Lai-Hung Lai, Matthijs Berghuis, Widianta Gomulya, Dmitry Dirin, Jih-Jen Wu, Maksym V. Kovalenko and Maria A. Loi, submitted.

6.1 **Introduction**

Solar energy to fuel conversion has attracted significant attention because of the abundant energy available from the sun. Hydrogen is an ideal energy buffer medium and energy carrier because: (i) the raw material (water) for producing hydrogen is abundant; (ii) it can be converted into electricity by fuel cells without producing pollutants;[1] (iii) in the last few years there have been seen rapid progresses in hydrogen storage.[2] Honda and Fujishima[3] first demonstrated PEC water splitting by employing TiO_2 as a photoanode, however the wide band gap of TiO_2 limits the photon absorption and results in low current density. Until now only materials for UV and visible light harvesting are available for PEC. In fact ambient and water stable narrow band gap semiconductors (for NIR light harvesting) are lacking. Most of the narrow band gap semiconductors such as Si, GaAs and InP require a protection layer to work in water environment,[4] and the protection layer makes the fabrication process longer and more expensive and still does not make the device stable.

Semiconducting single-walled carbon nanotubes (s-SWNT) are promising NIR light harvesting materials for photovoltaic applications due to their high carrier mobility and good air stability.[5, 6] Many researchers have employed unpurified (mixed semiconducting and metallic) tubes as a "scaffold" for sensitized solar cell[7] and electrocatalytic water splitting[8]. In these examples, SWNTs only play the role of enlarging the effective surface area instead of contributing to the photocurrent. In the previous chapter, we have successfully demonstrated the use of P3DDT-wrapped s-SWNT for H_2-evolving photocathode showing high stability and broad absorption range of the solar spectrum. Conjugated polymer wrapping has been demonstrated as an efficient way to select semiconducting tubes.[9] The electron/hole mobility of the s-SWNT strongly depends on the polymer species.[10, 11] The s-SWNT wrapped by P3DDT shows good hole transport properties with a mobility of 3.71 $cm^2\ V^{-1}\ s^{-1}$, however the electron mobility is lower. In contrast, s-SWNT wrapped by polyfluorene (PFO) shows ambipolar transport properties.[11]

The LUMO and HOMO of s-SWNT of diameter around 1 nm are in the range of -3.8 to -4.0 eV and -5.1 to –4.9 eV, respectively, depending on the precise diameter and chirality.[12] These energy levels are proper for proton reduction. As reported in the previous chapter by interfacing the p-type s-SWNT with n-type TiO_2, the photoelectrochemical properties are significantly improved. These results inspired us to fabricate a bulk heterojunction where the s-SWNTs form a hetrojuction with other

semiconductors. The high solubility of the polymer-wrapped s-SWNT in common organic solvents allows for processing them together with other solution-processed photocathode materials, such as P3HT:PCBM[13] and CdSe:P3HT[14]. In addition, in our previous study we found a more favourable charge separation in smaller diameter tubes due to the higher energy gap offset between the s-SWNT and the other semiconductors. Therefore, in this work we employ CoMoCAT SWNTs, which have relatively smaller diameter compared to HiPCO tubes.

In this chapter we report the study of the inclusion of polymer-wrapped s-SWNT into CdSe:P3HT hybrid photocathodes. The incorporation of s-SWNT into CdSe:P3HT blend is expected to give rise to the effective harvesting of the NIR spectral range as well as to improve the transport properties in the photocathode. This is the first report, to the best of our knowledge, demonstrating that the incorporation of s-SWNT into hybrid blends may trigger the formation of s-SWNT "scaffold" structure, which is a favorable structure for PEC water splitting due to the enlargement of the surface area and the improvement of the charge carrier transport.

6.2 Nanocrystals and single-walled carbon nanotubes

Semiconducting quantum dots (QDs) and s-SWNTs are zero and one-dimensional materials, respectively. Therefore, the optoelectronic properties of these low dimensional materials are strongly dependent on their size. The diameters of the tubes are determined by their (n,m) indices as follows, $d_t = \frac{a}{\pi}\sqrt{(n^2 + nm + m^2)}$, where $a = 0.246$ nm.[12] The first electronic transition energy can be approximated with the equation, $\Delta E_g^1 = 2\gamma_0 a_{cc}/d_t$, where $a_{cc} = 1.42\ \mathring{A}$ is the C-C bond length of the s-SWNT, $\gamma_0 = 2.9\ eV$ is the transfer integral between first-neighbor orbitals, and d_t is tube diameters.[15] The band gaps of tubes decrease as the inverse of the tube diameters. While for the QDs, the band gap is inversely proportional to the square of their diameters. The size of CdSe QDs used in this work is 3.3 nm, corresponding to a band gap of ~2.18 eV. While the SWNTs used have band gap of about 1 eV.

6.3 Selection of s-SWNT

The purity of the s-SWNT is important for fabrication of the hybrid photocathodes.[5] The metallic tubes may act as recombination centers, leading to photocathodes delivering very limited photocurrent and photovoltage. The co-existence of metallic and semiconducting tubes during

synthesis remains an obstacle for the application of SWNT in many electronic and optoelectronic applications. In the last ten years, several strategies to select s-SWNTs have been devised. Methods such as, encapsulation of SWNTs by DNA with specific sequences[16] and with surfactants followed by density gradient ultracentrifugation[17] have been developed, giving rise to the selection of several semiconducting SWNT chiralities. However, these water-based inks are difficult to be incorporated with other materials, especially with organic semiconductors, which are normally dissolved in organic solvents. Recently, conjugated polymers wrapping technique has been demonstrated as an efficient way to select semiconducting carbon nanotubes.[18] The s-SWNT/conjugated polymer hybrid formed by this self-assembly process can be dissolved in common organic solvents such as toluene or chloroform. The SWNT network field effect transistors (FETs) fabricated from this kind of dispersions show high carrier mobility (up to 30 $cm^2 V^{-1} s^{-1}$ for holes) and high on-off ratio ($>10^6$) in short channel length (10 μm) devices, indicating the absence of metallic tubes and superior charge carrier transport properties.[10, 11]

6.4 **Hybrid photocathodes**

The SWNT ink obtained with the polymer wrapping method can be used to fabricate hybrid photoelectrodes by simply mixing them with other co-sensitizers, such as CdSe QDs and P3HT. In chapter 5 we have demonstrated that CdSe and P3HT blend form a type II heterojunction, where P3HT extracts holes and CdSe extracts electrons that are further transferred to Pt which catalyzes the proton reduction.[14] Also, P3HT and s-SWNT have been reported to form a type II heterojunction, where s-SWNTs extract electrons from polymer.[19] The energy level diagrams of the different materials are shown in Figure 6.1(a). From the schematic it is evident that electrons can be injected from P3HT and CdSe to the s-SWNTs. To have better electron transport property, PFO wrapped s-SWNT are used instead of P3DDT wrapped one as has been reported in the previous chapter.[22] The PEC cell consists of the ternary blend based photocathode as a working electrode (WE), a saturated calomel electrode (SCE) as a reference electrode (RE), and a Pt coil counter electrode (CE); the schematic drawing of the cell is reported in Figure 6.1(b).

The absorption spectra of the CdSe QD solution, the s-SWNT solution and the CdSe:P3HT:s-SWNT (100:10:1 w/w/w) film are shown in Figure 6.2(a). Figure 6.2(a) shows that CdSe QDs have a clear excitonic peak at 570 nm, which indicates a band gap of about 2.2 eV. We can observe the

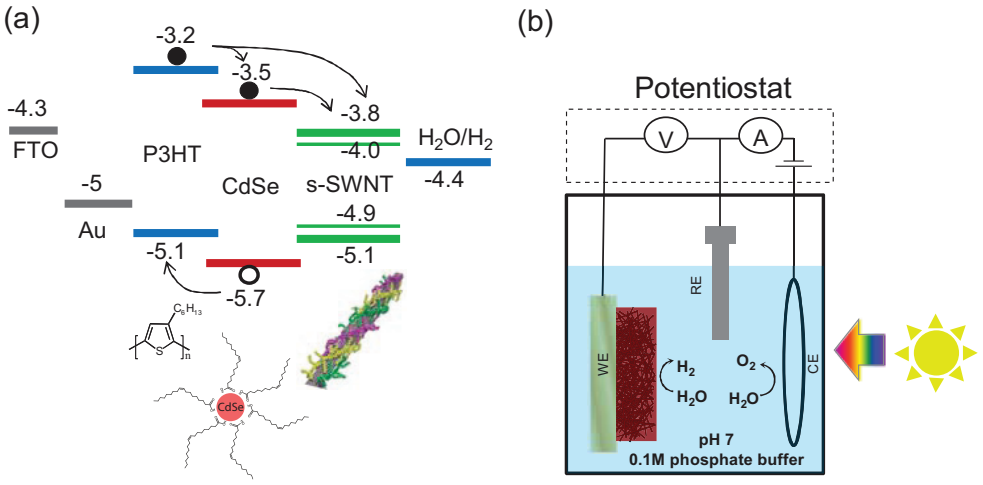

Figure 6.1. (a) Energy level diagrams of the materials composing the ternary blend photocathode. (b) Schematic drawing of the photoelectrochemical cell. The hybrid photocathode is the working electrode (WE), SCE is the reference electrode (RE) and a Pt coil is used as counter electrode (CE).

absorption peaks arising from the electronic transitions of different s-SWNT species as red line in Figure 6.2(a). SWNTs either have semiconducting or metallic properties, depending on their chirality determined by the unit vector indices (n,m). When $|n-m| = 3q$ (where q is an integer), the nanotubes are metallic or semi-metallic; otherwise they are semiconducting.[20] The first (E_{11}) and second (E_{22}) electronic transitions of CoMoCAT semiconducting SWNT result in absorption peaks in the spectral regions 1000-1400 nm and at 600-1000 nm, respectively. From the absorption measurement, we observe the presence of (7,5), (7,6), (8,6), (8,7), and (9,7) semiconducting species in the s-SWNT solution as shown in the yellow hexagons of Figure 6.2(b). The lack of absorption peaks contributed from metallic tubes (between 500-600 nm) indicates the high purity of s-SWNT in our solution. In ternary blend sample we observe a clear CdSe, P3HT, and s-SWNT absorption from the visible to the NIR spectral range.

The photocathodes were prepared by spin coating (using different rates from 1000 rpm to 4000 rpm) using a mixture of CdSe:P3HT:s-SWNT (in proportion 100:10:1 w/w/w) in chloroform. The films obtained are then treated with 1% 1,2-ethanedithiol (EDT) in acetonitrile for ligand exchange. After ligand exchange, the samples were washed several times with acetonitrile to remove the excess of ligands. A control experiment was performed with samples made without s-SWNT.

The morphological structure of these composite electrodes was investigated by SEM cross-sections (see Figure 6.3). The sample fabricated

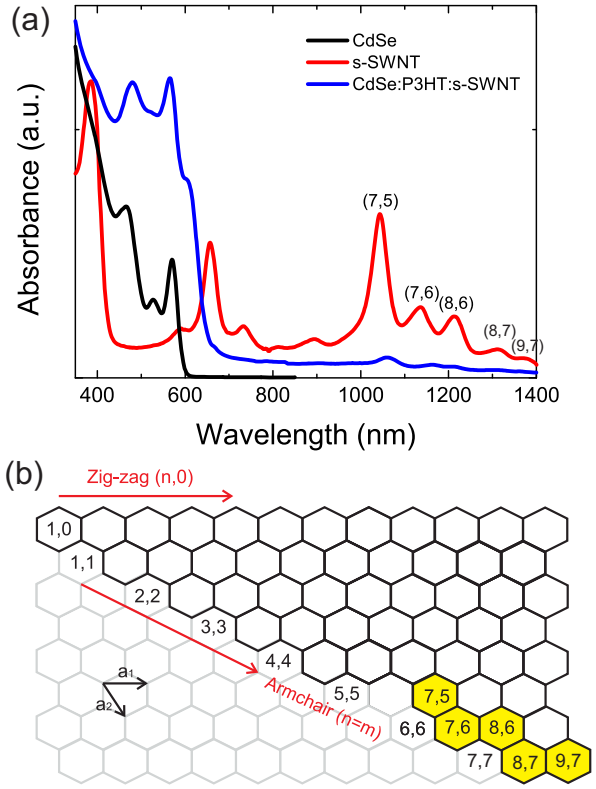

Figure 6.2. (a) Absorption spectra of CdSe colloidal solution, PFO wrapped SWNT (CoMoCAT) solution and ternary blend film composed of CdSe:P3HT:s-SWNT (100:10:1 w/w/w). (b) Chirality map of SWNTs selected by PFO. The presence of semiconducting species in the s-SWNT solution is underlined in the yellow hexagons.

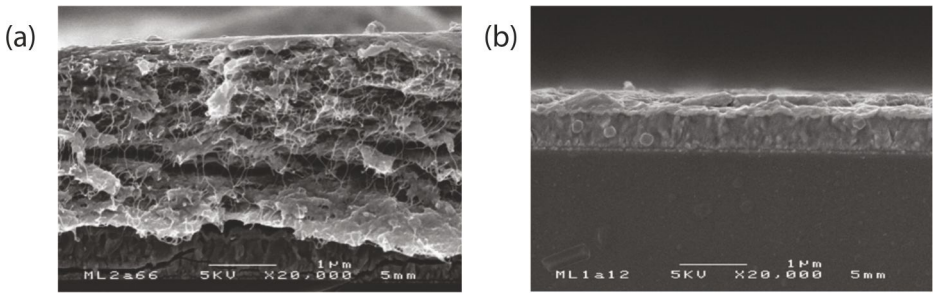

Figure 6.3. SEM Cross-section of (a) ternary blend with SWNT and (b) binary blend without SWNT.

with the SWNTs containing mixture at 1000 rpm spin coating rate shows a mesoporous-SWNT "scaffold" and a total thickness of about 2-3 μm (Figure 6.3(a)), while the sample fabricated on the same conditions but without

SWNT shows a smoother film structure of thickness smaller than 150 nm (see Figure 6.3(b)). This result suggests that the s-SWNTs are inclined to form porous aggregates in the ternary blend. To further understand the mechanism of the formation of s-SWNT "scaffold", we mix only two components i.e., s-SWNT:P3HT and s-SWNT:CdSe. The aggregates only can be found in s-SWNT:P3HT sample, indicating that the formation of the "scaffold" is induced by the interaction between the alkyl side-chain of the polymer wrapped s-SWNT and P3HT.

Before photoelectrochemical (PEC) measurement, on top of all samples was deposited a thin layer of Pt by photoreduction in 5 mM H_2PtCl_6 aqueous solution. The hybrid photocathodes were measured in a 3-electrode photoelectrochemical cell (Fig. 6.1(b)) with 0.1 M phosphate buffer (pH 7) as electrolyte. The J-V curves of the PEC cells based on the hybrid films with and without s-SWNT fabricated with different spin coating rates are shown

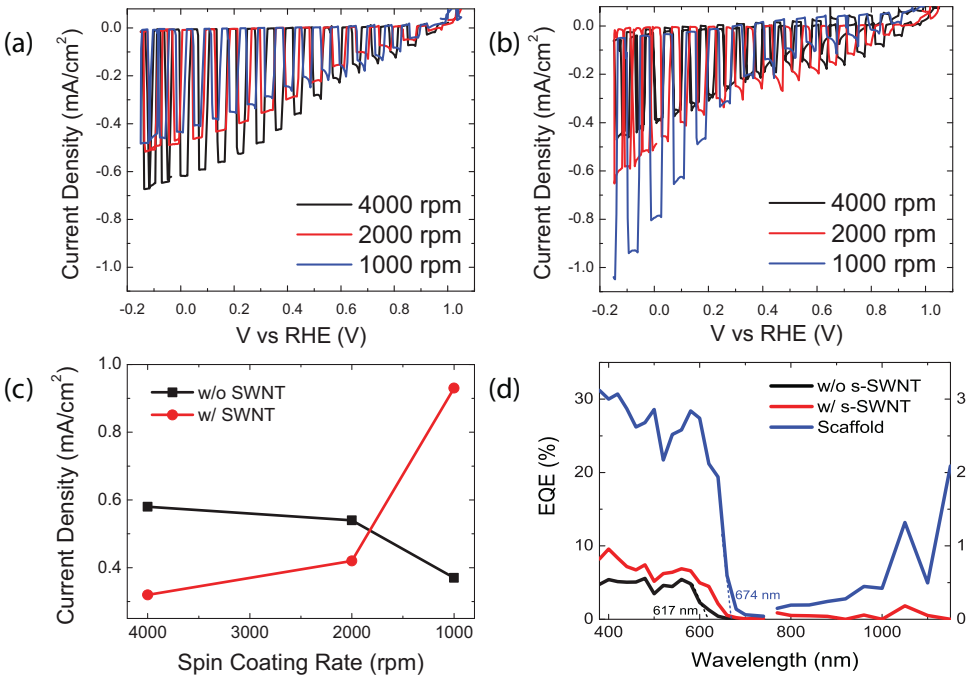

Figure 6.4. J-V characteristics of photocathodes without (a) and with (b) SWNTs fabricated with different spin coating rates. Measurements are performed under chopped light. (c) Summary of the photocurrent at 0 V_{RHE} obtained with photocathodes fabricated with different spin coating rates. (d) The *EQE* spectra of the photocathode without s-SWNT (black line) fabricated at 4000 rpm, of the photocathode fabricated with s-SWNT (red line) at 1000 rpm, and of a selected region "scaffold" of the last sample (blue line).

in Figure 6.4(a) and Figure 6.4(b), respectively. Figure 6.4(c) summarizes the photocurrent measured at 0 V_{RHE} as a function of the spin coating rate for the photocathode with and without SWNTs, where the photocathode without SWNTs shows lower photocurrent at lower spin coating rate (thicker film), while the opposite is observed for the photocathodes including s-SWNT. This can be explained by the fact that for the sample with s-SWNT the electronic transport is improved due to the relatively high electron mobility of the s-SWNT.

It is important to note that a much larger s-SWNT "scaffold" was observed in samples fabricated at lower spin coating rate, this occurrence makes us suspect that the s-SWNT "scaffold" has better photocatalytic properties than the planar film. Moreover, it is worthy to note that with the incorporation of SWNTs into the hybrid photocathode, the open circuit voltage (V_{oc}) keeps the same value as in the CdSe:P3HT device, indicating that the SWNTs provide a favorable carrier separation/transport instead of acting as recombination centers in the ternary blend.[21] The other reference devices, namely, the hybrid photocathode with only two components, i.e., s-SWNT:P3HT and s-SWNT:CdSe (Figure 6.6) were also measured. Both devices show much lower photocurrent compared to the three-component photocathode. It is also important to note that the V_{oc} of the CdSe:s-SWNT photocathode is reduced to ~0.1 V, which is much lower than all the other photocathodes, suggesting that CdSe and s-SWNT form a type I heterojunction.

The *EQE* spectra of the devices with optimized spin coating rate are shown in Figure 6.4(d). The s-SWNT hybrid photocathodes show the ability to harvest photons to perform proton reduction from 380 nm to 1150 nm. The *EQE* spectra are corrected for the absorption of water (see Figure 5.3). The missing *EQE* signal above 1150 nm is ascribed to the absorption by the 2.5 cm thick water medium, which allows only <5% of the light to pass through the electrochemical cell, resulting in low signal to noise ratio in the NIR. The *EQE* values of the s-SWNT based hybrid photocathodes are about 40% higher in the visible than that of the one without s-SWNT. Photos of the gas bubbles on the photocathode are shown in Figure 6.5.

In order to further investigate the PEC performance of the "scaffold" region, the *EQE* spectra were measured for the regions of the sample that exhibited higher "scaffold" concentration by masking the photocathode with a small aperture (black circle in Figure 6.5). The *EQE* value of the "scaffold" rich region are 6.5 times higher (from 0.2% to 1.5%) in the NIR and 3 times higher in the visible (from 10% to 30%) compared to that without the mask at the "scaffold" region (Figure 6.4(d)). This

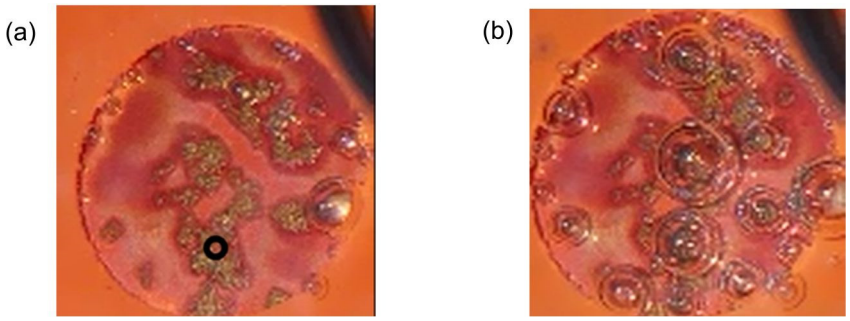

Figure 6.5. Photos of the ternary blend photocathode before (a) and after (b) light illumination. In (b) the generation of gas bubbles is evident.

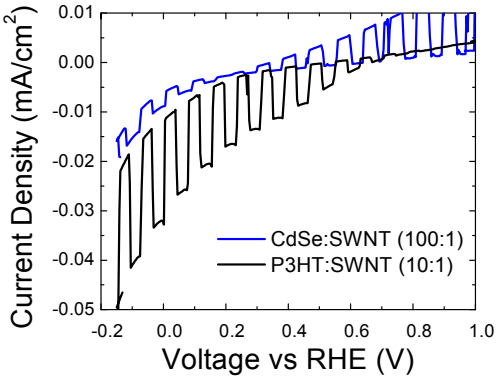

Figure 6.6. J-V characteristics of photocathodes composed by CdSe:s-SWNTs and P3HT:s-SWNTs.

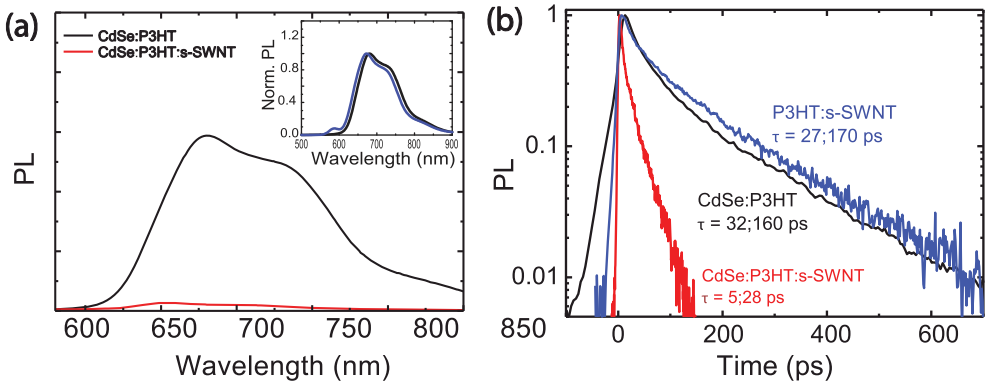

Figure 6.7. (a) Steady state spectra and (b) time-resolved PL decays of CdSe:P3HT(10:1) binary blend and of the CdSe:P3HT:s-SWNT (100:10:1) ternary blend film. Inset of (a) shows the steady state PL spectra of CdSe:P3HT (10:1) binary blend before (blue curve) and after (black curve) EDT ligand exchange.

measurements show that the porous SWNT "scaffold" improves the total performance of the photocathode. Note that the trace of the threshold edge of the *EQE* spectra red-shifts from 617 nm to 674 nm for the sample with s-SWNTs, which is ascribed to the better charge extraction from P3HT in this sample thanks to the s-SWNTs. This is further confirmed by the quenching of the P3HT emission for the sample containing s-SWNT (Figure 6.7).[22]

6.5 **Carrier dynamics**

The exciton separation dynamics can be further investigated by photoluminescence (PL) measurements. Figure 6.7(a) shows that the PL below 600 nm is contributed by the CdSe QD emission, which is quenched compared to the sample before ligand exchange (blue line in the inset of Figure 6.7(a)), in both binary and ternary blends after EDT ligand exchange. These measurements show that the charge separation in QDs is occurring in both binary and ternary blends after ligand exchange. Steady state PL measurements (Figure 6.7(a)) show that the excitation in the P3HT is further quenched by the addition of s-SWNTs into the CdSe:P3HT binary blend, which is a further signature of the efficient carrier transfer from the polymer to the s-SWNTs.[5, 19] The time resolved PL decays reported in Figure 6.7(b) show a strong reduction of the excitation lifetime, ~5 times shorter in the ternary blend (τ_1~ 5 ps and τ_2~ 28 ps) compared to the binary blend (τ_1~ 30 ps and τ_2~ 160 ps), which we believe is due to the charge transfer from P3HT towards s-SWNT as described in Figure 6.1(a).

The charge carrier transport dynamics was characterized by transient photocurrent measurements, which are reported in Figure 6.8(a). Transient photocurrent measurements were conducted at 0 V_{RHE} with a shutter opening and closing every 500 ms. When the light is switched on, the cathode transient photocurrent shows a step-like rise of the current till a level J_0 (-1.48 mA/cm^2) for the ternary blend sample, which tends to decrease toward the steady-state current $J_{s\text{-}s}$ (-1.41 mA/cm^2). This photocurrent response is 4 times higher than that of the binary blend, which was fabricated with the same condition except the addition of s-SWNT. The difference between the current density J_o and $J_{s\text{-}s}$ can be ascribed to charge recombination. However, an absence of anodic transient current was observed, indicating that the recombination of the minority carrier (hole) in CdSe QDs can be ruled out in this system.[14] Therefore the most plausible reason for the decay of the transient photocathodic current is the electron recombination.

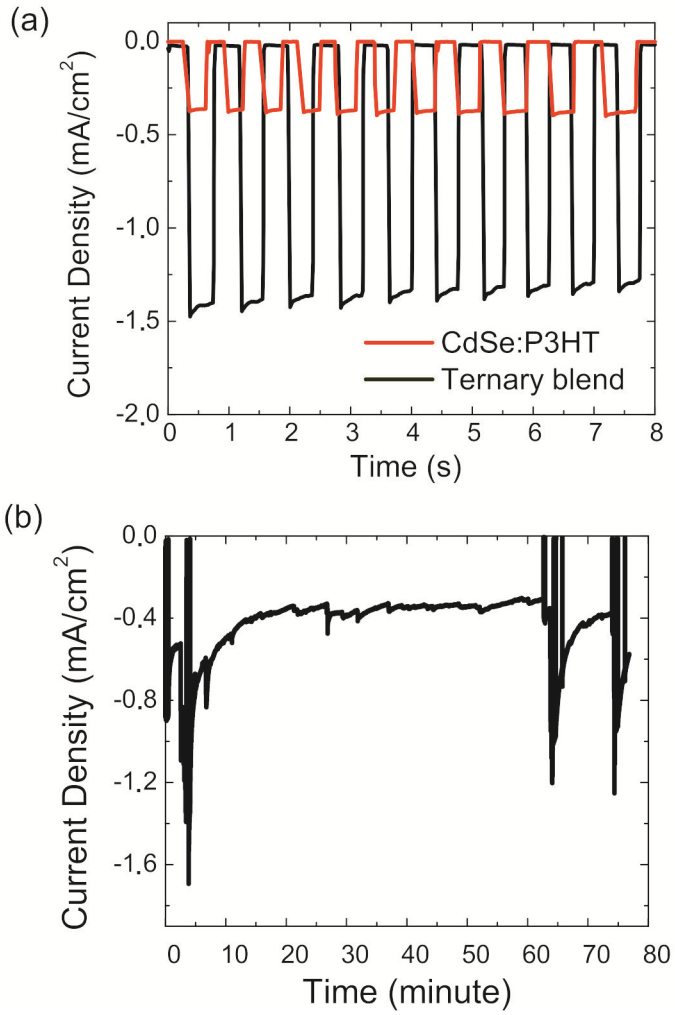

Figure 6.8. (a) Transient photocurrent of binary and ternary blend. (b) Stability of the ternary blend photocathode.

6.6 **Photocathode stability**

The study of the device stability is reported in Figure 6.8(b). Stable photocurrent for over 1 h of continuous measurement is observed. However, the gas bubble accumulation on the surface reduces the effective area of the photocathode, resulting in a decreasing of the photocurrent. After removing the bubbles from the surface by purging the electrolyte with N_2, the photocurrent almost recovers to the original value (~-1.3 mA cm^{-2}).

6.7 Conclusions

We have investigated the effects of the inclusion of s-SWNT in the CdSe:P3HT blend. A substantial increase of the light harvesting in the NIR spectral region was observed in the photocathode which uses the ternary blend. The SEM image showed that the aggregates in the hybrid film are composed of "scaffold" structures of high-density s-SWNT. The photocurrent of -1.3 mA cm^{-2} was achieved for the sample with s-SWNT inclusion, and an *EQE* of ~30% was obtained for the "scaffold" regions of the photocathode. Furthermore, the devices showed stable photocurrent for more than 1 h under continuous operation. This work highlights that the polymer-wrapped s-SWNTs are compatible with other solution-processable techniques for the fabrication of photoelectrodes for water splitting and they display a broad absorption of the solar spectrum and improved carrier transport properties.

6.8 Methods

Materials.

Sodium myristate (>98.0%, TCI), cadmium nitrate tetrahydrate (99.999%, Aldrich), selenium dioxide (SeO_2, 99.99%, Aldrich), 1-octadecene (ODE, 90%, Aldrich), oleic acid (OA, 90%, Aldrich), hexane (Aldrich), acetone (Aldrich), methanol (Aldrich) were used as received.

CdSe nanocrystal synthesis.

Cadmium myristate was prepared analogously to what reported in Ref. [23]. 6 mmol of sodium myristate dissolved in 240 mL of methanol and 0.617 g of cadmium nitrate in 40 mL of methanol. A second solution was added drop wise to the first one during continuous stirring. The white precipitate was filtered, washed two times with methanol and dried overnight at 50 °C in vacuum.

CdSe quantum dots (QDs) with zinc-blende structure were synthesized according to Ref. [24] with slight modifications. 34 mg (0.306 mmol) SeO_2, 173.5 mg (0.306 mmol) Cd myristate and 19.2 mL ODE were mixed, degassed 10 min at room temperature and quickly heated up to 240 °C. After 1 min of growth at 235-240 °C, 0.3 mL of oleic acid was injected and solution was cooled down to room temperature with water bath. QDs were washed three times with hexane/acetone, re-dissolved in chloroform and filtered through 0.2 μm filter.

Dispersion of SWNTs.

The preparation of polymer-wrapped s-SWNT was performed as in ref. 22. For all SWNTs dispersions, 6 mg of sooth and 6 mg of Poly(9,9-di-n-octylfluorenyl-2,7-diyl) (PFO) were added to 10 mL of toluene. The mixture was sonicated for 2 h in the cup horn of a high power sonicator (Misonix 3000) used at 90 W, during sonication the temperature of the sample was kept constant at 16 °C. Immediately after sonication, the dispersion was centrifuged with a ultracentrifuge Beckman Coulter (Optima XE-90; rotor: SW55Ti). For the sample used for the optical measurements the solution was centrifuged at 30000 rpm/195000 g for 2 h, and for several hours (with one step at 195000 g and a second step at 368000 g) for the samples used to fabricate the photocathodes. For the samples used to fabricate the photocathode, the pellet obtained with the second ultracentrifugation was re-dispersed in 1 mL toluene.

Hybrid photocathode fabrication.

Fluorine-doped tin oxide (FTO) substrates were cleaned with soap and water and sonicated in deionized water, acetone and isopropyl alcohol in an ultrasonic bath. Then 7 nm of Cr and 100 nm thick Au film were evaporated on the substrate. The toluene was removed in s-SWNT solution by rotary evaporator before mixing with CdSe and P3HT. The CdSe QDs (30 mg/ml) were mixed with P3HT (Plexcore® OS 2100, regioregular, average Mn 54,000-75,000) and s-SWNT in chloroform. To obtain the s-SWNT aggregations "scaffold", the hybrid solution was stirred at 50 ^{o}C on the hot plate for 24 h before spin casting. The hybrid film was spin casted on the FTO/Cr/Au substrates. Then the 1% 1,2-ethanedithiol (EDT) solution in acetonitrile (v/v) was drop-casted on the hybrid film and left to react for 1 min before spin-drying. The samples were further rinsed with acetonitrile and spin-dried. After fabrication, the devices were annealed at 110 ^{o}C for 20 min. Pt was deposited on top of the hybrid layer by photoreduction in 5 mM $H_2PtCl_6 \cdot 6H_2O$ aqueous solution with a pH value of 11 tuned by 2 M NaOH at potential of -0.627 V vs SCE for 30 s under 1 sun illumination.

Characterization.

J-V curves were measured with a SP-200 Bio-Logic potentiostat equipped with an electrochemical impedance spectroscopy analyzer. Solar cells measurements were performed under 100 mW/cm^2 AM 1.5G conditions obtained with a solar simulator (SF150 class A, Sciencetech) calibrated by a Si reference cell (SRC-1000-RTD-QZ, VLSI Standards Incorporated). External quantum efficiencies (*EQE*) measurements were performed at short circuit voltage using a 250 W quartz tungsten halogen lamp (6334NS, Newport

with lamp housing 67009, Newport), and wavelength selection was obtained with a set of band-pass filters (Thorlabs) with full width half maximum (FWHM) of 10 ± 2 nm from 400 nm to 1300 nm and FWHM of 12 ± 2.4 nm from 1300 nm to 1400 nm. PD300 and PD300IR (Ophir Optics) are used as calibrated photodiodes. The photocathode was characterized by three-electrode electrochemical cells composed of working electrode, reference electrode (saturated calomel electrode (SCE)), and counter electrode (Pt coil) in 0.1 M NaH_2PO_4 phosphate buffer with a pH value of 7 tuned by 2 M NaOH. The film thickness measurements were performed using a Veeco Dektak 6M profilometer. Absorbance spectra were measured by UV-3600 UV-Vis-NIR spectrophotometer (Shimadzu Scientific Instruments). SEM images were recorded using a JEOL 6320F Field Emission microscope working at 5 kV and a beam current of 1×10^{-10} A. The working distance was 5 mm. Prior to imaging by SEM, the samples were coated with 3 nm Pt/Pd (80/20). Photoluminescence measurements were performed by exciting the samples at 400 nm by the second harmonic of a mode-locked Ti:Sapphire laser delivering pulses of 150 fs at a repetition frequency of 76 MHz. The steady state PL was recorded using a Si CCD detector, while time-resolved PL measurements were recorded by a Hamamatsu streak camera working in synchroscan mode. All PL spectra were corrected for the spectral response of the setup.

6.9 References

[1] B. C. Steele, A. Heinzel, *Nature* **2001**, *414*, 345-352.
[2] K. J. Jeon, H. R. Moon, A. M. Ruminski, B. Jiang, C. Kisielowski, R. Bardhan, J. J. Urban, *Nat. Mater.* **2011**, *10*, 286-290.
[3] A. Fujishima, K. Honda, *Nature* **1972**, *238*, 37-38.
[4] S. Hu, M. R. Shaner, J. A. Beardslee, M. Lichterman, B. S. Brunschwig, N. S. Lewis, *Science* **2014**, *344*, 1005-1009.
[5] S. Ren, M. Bernardi, R. R. Lunt, V. Bulovic, J. C. Grossman, S. Gradecak, *Nano Lett.* **2011**, *11*, 5316-5321.
[6] M. Gong, T. A. Shastry, Y. Xie, M. Bernardi, D. Jasion, K. A. Luck, T. J. Marks, J. C. Grossman, S. Ren, M. C. Hersam, *Nano Lett.* **2014**, *14*, 5308-5314; F. Schöppler, C. Mann, T. C. Hain, F. M. Neubauer, G. Privitera, F. Bonaccorso, D. Chu, A. C. Ferrari, T. Hertel, *J. Phy. Chem. C* **2011**, *115*, 14682-14686; S. L. Guillot, K. S. Mistry, A. D. Avery, J. Richard, A. M. Dowgiallo, P. F. Ndione, J. van de Lagemaat, M. O. Reese, J. L. Blackburn, *Nanoscale* **2015**, *7*, 6556-6566; D. J. Bindl, M. S. Arnold, *J. Phy. Chem. C* **2013**, *117*, 2390-2395.
[7] I. Robel, B. A. Bunker, P. V. Kamat, *Adv. Mater.* **2005**, *17*, 2458-2463; C. Schulz-Drost, V. Sgobba, C. Gerhards, S. Leubner, R. M. Krick Calderon, A. Ruland, D. M. Guldi, *Angew. Chem. Int. Ed.* **2010**, *49*, 6425-6429; D. M. Guldi, G. M. Rahman, M. Prato, N. Jux, S. Qin, W. Ford, *Angew. Chem. Int. Ed.* **2005**, *44*, 2015-2018; V. Sgobba, G. M. A. Rahman, D. M. Guldi, N. Jux, S. Campidelli, M. Prato, *Adv. Mater.* **2006**, *18*, 2264-2269; T. Hasobe, S. Fukuzumi, P. V. Kamat, *J. Phys. Chem. B* **2006**, *110*, 25477-25484; P. Brown, K. Takechi, P. V. Kamat, *J. Phys. Chem. C* **2008**, *112*, 4776-4782; S. R. Jang, R. Vittal, K. J. Kim, *Langmuir* **2004**, *20*, 9807-9810; A. Kongkanand, R. M. Dominguez, P. V. Kamat, *Nano Lett.* **2007**, *7*, 676-680.
[8] X. Zou, X. Huang, A. Goswami, R. Silva, B. R. Sathe, E. Mikmekova, T. Asefa, *Angew. Chem. Int. Ed. Engl.* **2014**, *53*, 4372-4376; M. Gong, W. Zhou, M. C. Tsai, J. Zhou, M. Guan, M. C. Lin, B. Zhang, Y. Hu, D. Y. Wang, J. Yang, S. J. Pennycook, B. J. Hwang, H. Dai, *Nat. Commun.* **2014**, *5*, 4695; F. M. Toma, A. Sartorel, M. Iurlo, M. Carraro, P. Parisse, C. Maccato, S. Rapino, B. R. Gonzalez, H. Amenitsch, T. Da Ros, L.

Casalis, A. Goldoni, M. Marcaccio, G. Scorrano, G. Scoles, F. Paolucci, M. Prato, M. Bonchio, *Nat. Chem.* **2010**, *2*, 826-831.
[9] S. K. Samanta, M. Fritsch, U. Scherf, W. Gomulya, S. Z. Bisri, M. A. Loi, *Acc. Chem. Res.* **2014**, *47*, 2446-2456.
[10]S. Z. Bisri, J. Gao, V. Derenskyi, W. Gomulya, I. Iezhokin, P. Gordiichuk, A. Herrmann, M. A. Loi, *Adv. Mater.* **2012**, *24*, 6147-6152; W. Gomulya, V. Derenskyi, E. Kozma, M. Pasini, M. A. Loi, *Adv. Func. Nater.* **2015**, *25*, 5858-5864.
[11]V. Derenskyi, W. Gomulya, J. M. Rios, M. Fritsch, N. Frohlich, S. Jung, S. Allard, S. Z. Bisri, P. Gordiichuk, A. Herrmann, U. Scherf, M. A. Loi, *Adv. Mater.* **2014**, *26*, 5969-5975.
[12]M. S. Dresselhaus, G. Dresselhaus, R. Saito, *Carbon* **1995**, *33*, 883-891.
[13]T. Bourgeteau, D. Tondelier, B. Geffroy, R. Brisse, R. Cornut, V. Artero, B. Jousselme, *ACS Appl. Mat. Interfaces* **2015**, *7*, 16395-16403; T. Bourgeteau, D. Tondelier, B. Geffroy, R. Brisse, C. Laberty-Robert, S. Campidelli, R. de Bettignies, V. Artero, S. Palacin, B. Jousselme, *Energy Sustain Soc* **2013**, *6*, 2706-2713.
[14]L. H. Lai, W. Gomulya, M. Berghuis, L. Protesescu, R. J. Detz, J. N. Reek, M. V. Kovalenko, M. A. Loi, *ACS Appl. Mat. Interfaces* **2015**, *7*, 19083-19090.
[15]J.-C. Charlier, X. Blase, S. Roche, *Rev. Mod. Phys.* **2007**, *79*, 677-732.
[16]X. Tu, S. Manohar, A. Jagota, M. Zheng, *Nature* **2009**, *460*, 250-253.
[17]S. Ghosh, S. M. Bachilo, R. B. Weisman, *Nat. Nanotechnol.* **2010**, *5*, 443-450; M. S. Arnold, A. A. Green, J. F. Hulvat, S. I. Stupp, M. C. Hersam, *Nat. Nanotech.* **2006**, *1*, 60-65; M. C. Hersam, *Nat. Nanotechnol.* **2008**, *3*, 387-394.
[18]W. Gomulya, G. D. Costanzo, E. J. de Carvalho, S. Z. Bisri, V. Derenskyi, M. Fritsch, N. Frohlich, S. Allard, P. Gordiichuk, A. Herrmann, S. J. Marrink, M. C. dos Santos, U. Scherf, M. A. Loi, *Adv. Mater.* **2013**, *25*, 2948-2956.
[19]J. M. Holt, A. J. Ferguson, N. Kopidakis, B. A. Larsen, J. Bult, G. Rumbles, J. L. Blackburn, *Nano Lett.* **2010**, *10*, 4627-4633; Y. Kanai, J. C. Grossman, *Nano Lett.* **2008**, *8*, 908-912; D. J. Bindl, N. S. Safron, M. S. Arnold, *ACS Nano* **2010**, *4*, 5657-5664; S. D. Stranks, C. Weisspfennig, P. Parkinson, M. B. Johnston, L. M. Herz, R. J. Nicholas, *Nano Lett.* **2011**, *11*, 66-72.
[20]X. Lu, Z. Chen, *Chem. Rev.* **2005**, *105*, 3643-3696.
[21]F. Gao, Z. Li, J. Wang, A. Rao, I. A. Howard, A. Abrusci, S. Massip, C. R. McNeill, N. C. Greenham, *ACS Nano* **2014**, *8*, 3213-3221.
[22]D. Jarzab, F. Cordella, M. Lenes, F. B. Kooistra, P. W. Blom, J. C. Hummelen, M. A. Loi, *J. Phys. Chem. B* **2009**, *113*, 16513-16517.
[23]Y. A. Yang, H. Wu, K. R. Williams, Y. C. Cao, *Angew. Chem. Int. Ed.* **2005**, *44*, 6712-6715.
[24]O. Chen, X. Chen, Y. Yang, J. Lynch, H. Wu, J. Zhuang, Y. C. Cao, *Angew. Chem. Int. Ed.* **2008**, *47*, 8638-8641.